Letter

Optimal superconductivity in twisted bilayer WSe_2 where the Van Hove singularity crosses half-filling

Michał Zegrodnik,[1,*] Waseem Akbar,[1] Andrzej Biborski,[1] and Louk Rademaker[2,3]

[1]*Academic Centre for Materials and Nanotechnology, AGH University of Krakow, Al. Mickiewicza 30, 30-059 Krakow, Poland*

[2]*Department of Theoretical Physics, University of Geneva, CH-1211 Geneva, Switzerland*

[3]*Institute-Lorentz for Theoretical Physics, Leiden University, P.O. Box 9506, Leiden NL-2300, The Netherlands*

(Received 2 June 2025; accepted 28 January 2026; published 25 March 2026)

The recent discovery of unconventional superconductivity has pointed to twisted WSe_2 bilayer as a versatile platform for studying the correlated and topological phases of matter. Here, we analyze the effect of the displacement field and electron interactions on the formation of a topological paired state in twisted WSe_2. Our approach is based on the effective single band t-J-U model supplemented with intersite Coulomb interaction term and treated within the Gutzwiller approximation. We show that the superconducting phase is stabilized in a small range of displacement fields where the Van Hove singularity crosses half-filling, which is in qualitative agreement with recent experimental data. According to our analysis, such a circumstance comes as a result of a subtle interplay between the large density of states of the Van Hove singularity, in combination with the renormalization effects that appear in the weak-to-moderate correlation regime. The two factors create favorable conditions for the superconducting pairing only in a small area of the phase diagram.

DOI: 10.1103/pkf3-fkv4

Introduction. Transition-metal dichalcogenide bilayers have recently attracted a significant amount of interest due to their rich physics and exceptional tunability. It has been established experiementally that those systems host a number of correlated and topological states such as Mott insulators [1,2], magnetically ordered states [3,4], generalized Wigner crystals [5–9], quantum anomalous and spin quantum anomalous Hall states [4,10,11], and Kondo effects [12]. Moreover, in recent years signatures of unconventional superconducting (SC) state have been reported, first by Wang *et al*. for the case of the twisted WSe_2 bilayer ($tWSe_2$) [2]. It has been suggested that for this system two superconducting domes reside on both sides of a Mott insulating state, which is located at half-filling similarly to that in the well-known cuprates [13] or twisted bilayer graphene [14,15]. Interestingly, strong evidence of the paired state in $tWSe_2$ has been shown in very recent experimental papers, which, however, report one SC dome close to or at the half-filling for a certain range of displacement fields [16,17].

Depending on the twist angle (θ) between the two WSe_2 monoatomic layers, a moiré pattern emerges, which leads to the creation of a mini-Brillouin zone and, most importantly, to flat electronic bands [18]. This points to a significant role played by electron-electron interactions. It is believed that $tWSe_2$ is in the moderately correlated regime, with the on-site Coulomb integral being comparable to the flat band width ($U \approx W$) [2,19]. However, the actual strength of the electron-electron correlations is influenced by the twist angle and the dielectric environment of the sample. The experimental absence of the Mott insulating state at half-filling in Ref. [17] indicates that most probably a weak-to-moderate correlation regime ($U \lesssim W$) has been achieved in this particular study. Moreover, it has been established that the paired state emerges only in a relatively small range of displacement fields and band fillings, whose exact location depends on the twist angle.

The original experimental report as well as the most recent ones related with SC state in $tWSe_2$ has motivated theoretical analysis that considered effective single- and multiband models as well as different forms of pairing mechanisms [20–32]. Many of the those considerations lead to a mixed singlet and triplet symmetry of the order parameter, due to the presence of the Ising-type spin-orbit coupling in the system. Both the theoretical study and the experimental reports point to the role of the Van Hove singularity (VHS) in the stabilization of the paired state. However, the physical mechanism that determines the characteristic form of the phase diagram is still under ongoing debate and has not been completely resolved so far.

In our previous study, we have employed an effective single-band t-J-U model to the description of SC state of $tWSe_2$, which leads to the stability of a topological mixed $d + id$ and p-ip pairing scenario [23,33]. Within such a description, the single-particle physics is described by a tight binding Hamiltonian with complex hoppings that incorporate the spin-valley locking in the system. Here, we extend our previous considerations by supplementing the Hamiltonian with an *intersite Coulomb interaction term*. We focus on the effect of the displacement field in the formation of the paired

*Contact author: michal.zegrodnik@agh.edu.pl

Published by the American Physical Society under the terms of the Creative Commons Attribution 4.0 International license. Further distribution of this work must maintain attribution to the author(s) and the published article's title, journal citation, and DOI.

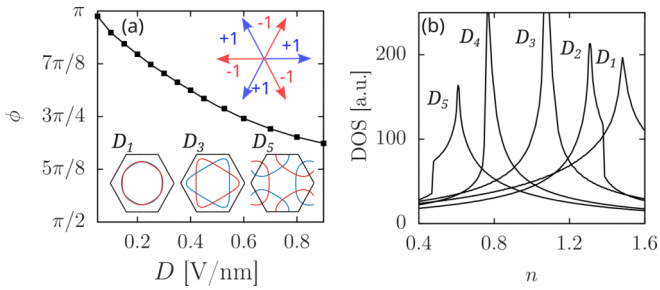

FIG. 1. (a) Phase factor ϕ as a function of displacement field, D, together with spin-up (blue) and spin-down (red) Femi surfaces at half-filling for selected values of D (inset). In the upper right corner, we provide the $\nu_{ij} = \pm 1$ factor corresponding to the six nearest neighbors [cf. Eq. (1)]. (b) Density of states at the Fermi level as a function of band filling for selected values of the displacement field $D_l \in \{0.05,\ 0.2,\ 0.3,\ 0.45,\ 0.6\}$ V/nm, for $l = 1, 2, 3, 4, 5$, respectively.

state in order to discuss the obtained results in the view of the most recent experimental findings. In particular, our main aim here is to reconstruct one of the principal features of the $tWSe_2$, namely, the appearance of an unconventional superconducting state in a relatively small range of displacement fields (D) and band fillings (n) [16,17]. In our study, we apply the Gutzwiller approximation based on which we analyze in detail the electron-correlation-induced renormalization of particular energy terms in the context of the SC state stabilization. As we show explicitly, in the regime of weak-to-moderate correlations, the renormalization effects create favorable conditions for the SC pairing in close proximity of the half-filled situation. This effect, together with the Van Hove singularity evolution induced by the displacement field, determines the stability regime of the SC state in the (n, D) phase diagram.

Model and method. We employ the moiré t-J-U model supplemented with the intersite Coulomb repulsion term, i.e.,

$$\begin{aligned}\hat{H} =& t \sum_{\langle ij\rangle\sigma} e^{i\sigma\nu_{ij}\phi}\, \hat{c}^{\dagger}_{i\sigma}\hat{c}_{j\sigma} \\ &+ J \sum_{\langle ij\rangle}{}' \left(\hat{S}^z_i \hat{S}^z_j + \frac{1}{2} e^{i2\nu_{ij}\phi} \hat{S}^+_i \hat{S}^-_j + \frac{1}{2} e^{-i2\nu_{ij}\phi} \hat{S}^-_i \hat{S}^+_j \right) \\ &+ U \sum_i \hat{n}_{i\uparrow}\hat{n}_{i\downarrow} + V \sum_{\langle ij\rangle}{}' \hat{n}_i \hat{n}_j, \end{aligned} \tag{1}$$

where $\sigma = \pm 1$ represents spin up/down, $\hat{c}^{\dagger}_{i\sigma}$ and $\hat{c}_{i\sigma}$ are the creation and annihilation operators for electron with spin σ at site i of a triangular lattice, $\langle i, j\rangle$ correspond to nearest neighbors, S^z_i, S^+_i, and S^-_i are the spin-$\frac{1}{2}$ z component and rising and lowering operators, respectively, $\hat{n}_{i\sigma}$ is the occupancy operator, and $\hat{n}_i = \sum_\sigma \hat{n}_{i\sigma}$. The primed summation means that each bond between the lattice sites appears only once. The subsequent terms of the above Hamiltonian correspond to electron hopping, intersite exchange interaction, and intra/intersite Coulomb repulsion. The phase factors of the exponents have an alternating sign introduced by $\nu_{ij} = \pm 1$, which depends on the bond direction (cf. inset of Fig. 1). The resultant spin- and direction-dependent complex hoppings account for the Ising-type spin-orbit coupling in the system. As shown in Refs. [2,19], the single-particle part constitutes an effective description of the flat moiré band of twisted WSe_2/WSe_2 homobilayer. It should be noted that in the experimental situation the $tWSe_2$ structure is usually placed in between two electrodes that allow to control both the electron concentration (n) and the displacement field (D) in an *in situ* manner. The effect of the latter tunes the spin-valley splitting and enters the effective model via a D-dependent t and ϕ, which have been calculated for the twist angle of $\theta = 5.08^\circ$ in Ref. [2] and are used by us here. For the sake of completeness in Fig. 1, we provide the D dependence of ϕ as well as Fermi surfaces and density of states as a function of band filling for selected values of displacement field.

Motivated by the experimental result provided in Ref. [17], we focus on the weak-to-moderate correlation regime ($U/W \lesssim 1$) by taking $U = 80$ meV, where the bandwidth is $W \approx 90$ meV. The value of the exchange interaction integral is set to $J = 4t^2/U$. We apply the Gutzwiller approximation method, which takes into account the electron-electron interactions above the level of a standard mean-field approach. At the same time, the considered method allows us to access the renormalization factors corresponding to subsequent energy terms appearing in our Hamiltonian and analyze them in the context of the SC state formation. The considered variational wave function of the Gutzwiller type has the following form $|\Psi_G\rangle = \hat{P}|\Psi_0\rangle$, where $|\Psi_0\rangle$ is the uncorrelated (mean-field) state and $\hat{P}$ denotes the correlation operator, i.e.,

$$\hat{P} = \prod_i \sum_\Gamma \lambda_{i,\Gamma} |\Gamma\rangle_{i\,i}\langle\Gamma|, \tag{2}$$

while $|\Gamma\rangle$ are states from the local basis $\{|\emptyset\rangle, |\uparrow\rangle, |\downarrow\rangle, |\uparrow\downarrow\rangle\}$ and $\lambda_{i,\Gamma}$ represent variational parameters determined via energy minimization. Since we consider a homogeneous system without magnetic or charge ordering, we take $\lambda_{i,\uparrow\downarrow} \equiv \lambda_{\uparrow\downarrow}$, $\lambda_{i,\uparrow} = \lambda_{i,\downarrow} \equiv \lambda_s$, and $\lambda_{i,\emptyset} \equiv \lambda_\emptyset$.

It is important to note that, when it comes to stabilization of the superconducting state, the exchange interaction term (J) and the intersite Coulomb interaction term (V) have positive and negative effects, respectively. Within the Gutzwiller approximation, the expectation values in the $|\Psi_G\rangle$ state of the two mentioned terms is the following:

$$\begin{aligned} E_J =& \lambda_s^4 J \sum_{\langle ij\rangle}{}' \Bigg(\frac{1}{2} \sum_\sigma e^{i\sigma 2\phi_{ij}} \langle \hat{c}^{\dagger}_{i\sigma}\hat{c}_{i\bar{\sigma}}\hat{c}^{\dagger}_{j\bar{\sigma}}\hat{c}_{j\sigma}\rangle_0 \\ &+ \frac{1}{4} \sum_{\sigma\sigma'} \sigma\sigma' \big(\langle \hat{n}_{i\sigma}\hat{n}_{j\sigma'}\rangle_0 - n_s^2 \big) \Bigg), \\ E_V =& V \sum_{\langle ij\rangle}{}' \big(g_v^2 \langle \hat{n}_i \hat{n}_j\rangle_0 - (1 - g_v^2) n_s^2 \big), \end{aligned} \tag{3}$$

where $g_v = (1 - (2 - \lambda^2_{\uparrow\downarrow})n_s)/(1 - n_s)$, $n_{i\uparrow} = n_{i\downarrow} \equiv n_s$, $n_{i\sigma} = \langle \hat{n}_{i\sigma}\rangle_0$, and $\langle \hat{o}\rangle_0$ refers to an expectation value of operator $\hat{o}$ in the $|\Psi_0\rangle$ state. As one can see, the expectation value of a given energy term in the correlated state, $|\psi_G\rangle$, can be expressed in terms of the expectation values in the uncorrelated state, $|\psi_0\rangle$. However, factors λ_s^4 and g_v^2 renormalize the coupling constants J and V, respectively. Therefore, the

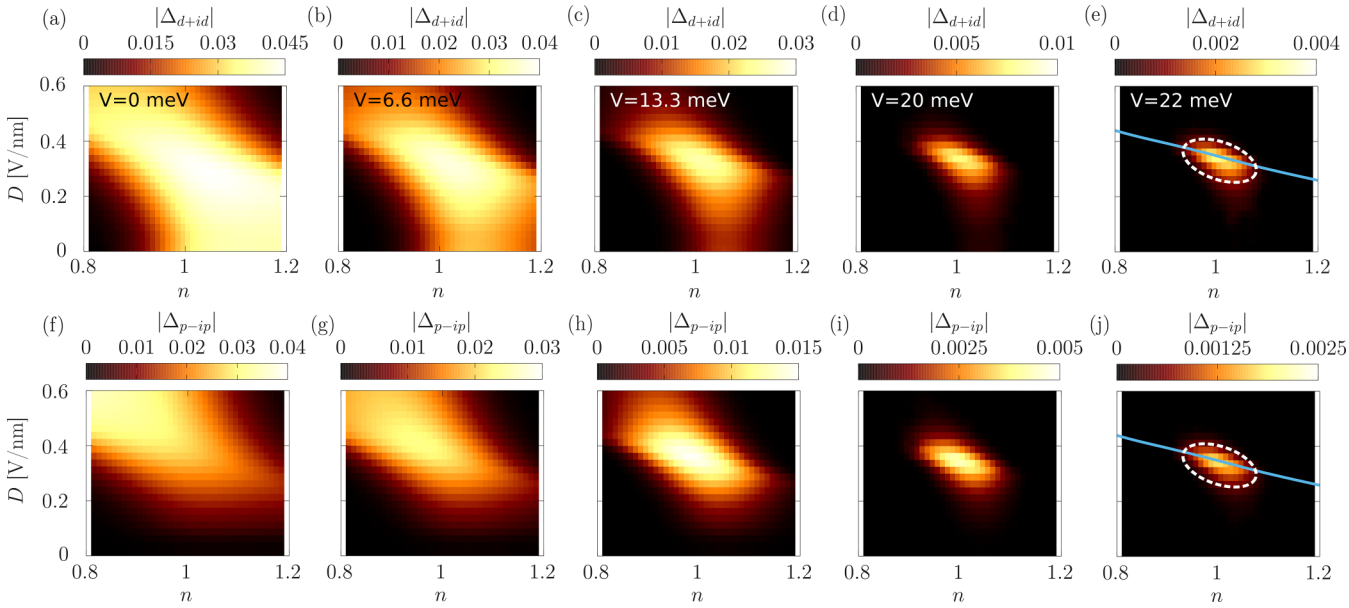

FIG. 2. Symmetry resolved superconducting gap amplitudes corresponding to the obtained mixed spin-singlet $d + id$ and spin-triplet $p - ip$ paired state as a function of band filling n and displacement field D for gradually increasing value of the intersite Coulomb repulsion V(a − j). The on-site Coulomb repulsion and the exchange interaction parameters are set to $U = 80$ meV and $J = 4t^2/U$, respectively. The solid blue line in panels (e) and (j) mark the evoulution of the Van Hove singularity across the phase diagram. The white dashed line is a guide to the eye denoting the stability range of the SC state.

relative balance between the two energy terms is going to be affected by the significant on-site Coulomb repulsion via the renormalization factors possibly having a decisive influence on the stabilization of the superconducting state.

To determine the values of the real-space superconducting gap amplitudes in the correlated state, $\Delta_{ij}^{\sigma\bar{\sigma}} = \langle \hat{c}_{i\sigma}^{\dagger} \hat{c}_{j\bar{\sigma}}^{\dagger} \rangle_G$, we apply the effective Hamiltonian scheme [34] and then extract the symmetry-resolved SC gaps [23], which allow us to analyze the principal features of the paired state. Also, following Bünemann *et al.*, we impose an additional condition to the correlation operator, which reduces the complexity of the numerical calculations [35]. More details related to the applied theoretical approach are provided in the Supplemental Material [36], which includes Refs. [37–50]. In the following, we refer to the average number of electrons per lattice site as band filling $n = 2n_s$.

Results. In order to discuss our theoretical approach in the context of the available experimental data, we calculate the symmetry-resolved SC amplitudes across the (n, D) diagram. In Fig. 2, we provide the results obtained for the gradually increasing value of the intersite Coulomb repulsion, V. Our calculations lead to the stabilization of a mixed $d + id$ (singlet) and p-ip (triplet) paired state. Singlet-triplet mixing has also been reported in other theoretical descriptions of $tWSe_2$ [21,22,25,30,32] and is a straightforward consequence of the spin-valley locking as we discuss in more detail in the Appendix and/or Supplemental Material [36]. As one can see, for the $V = 0$ case the SC state is relatively robust, with the spin-singlet pairing dominating the low displacement field regime and gradually increasing contribution resulting from the triplet component as D increases. Such robust SC state covering a significant area of the phase diagram is in contradiction with the experimental situation. However, as the value of V is increased, the stability area of the paired state shrinks. It should be noted that the negative effect of the V term on the pairing has been previously reported in other theoretical considerations [51–53]. For $V = 22$ meV, the SC phase covers only a small part of the (n, D) plane, which is located in the proximity of the half-filled situation, and for $D \approx 0.2$–0.4 V/nm. The SC phase shown in Figs. 2(e) and 2(j) is characterized by a Chern number $C = \pm 4$ indicating a topological character. The sign change of C appears exactly at the Van Hove singularity line, which is due to the transition from the electronlike to holelike Fermi surfaces. For more details related with the topological features, see the Appendix and/or Supplemental Material [36]. It should be noted that a similar form of the phase diagram has recently been reported experimentally for $tWSe_2$ in Ref. [17]. However, due to uncertainty in experimental determination of band filling, it is not completely clear whether the SC phase stability range has reached the half-filled situation. Another experimental report has shown the SC phase stability at half-filling but in very low displacement field range [16].

In order to analyze why the particular small area of the (n, D) plane seen in Figs. 2(e) and 2(j) creates favorable conditions for the SC state to be stable, we first study the evolution of Van Hove singularity across the phase diagram. The solid blue line marks the band fillings that for a given value of D correspond to the Van Hove singularity being located at the Fermi level. As one can see, the area covered by the SC state is located around the Van Hove singularity line. Such an effect is expected since high values of the density of states at the Fermi energy stabilize superconductivity in the weak-coupling theory. The second effect that is of significant importance here originates from the electron-electron correlations. In Fig. 3, we provide the (n, D) dependence of the g_v^2 and λ_s^4 factors,

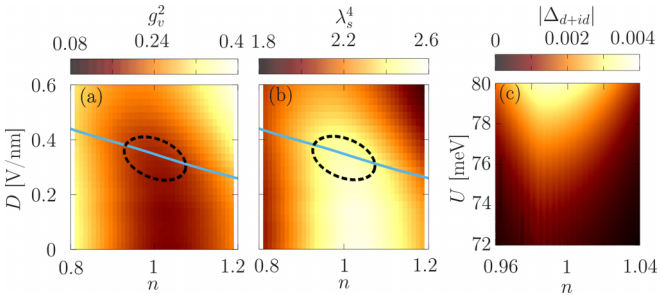

FIG. 3. The g_v^2 [panel (a)] and λ_s^4 [panel (b)] factors that renormalize the intersite Coulomb interaction term and the exchange interaction term [cf. Eq. (3)], respectively, as a function of n and D. The blue line marks the Van Hove singularity evolution across the phase diagram. The black dashed line corresponds to the stability of the SC state as in Figs. 2(e) and 2(j). Note that SC phase is located at the crossing of the Van Hove singularity line and the area where the renormalization is the strongest. (c) The SC gap as a function of U and n for $D = 0.35$ V/nm with $J = 4t^2/U$, $V = U/3.635$. We provide only the singlet component since the triplet one shows the same behavior but is approximately twice smaller.

which renormalize the intersite Coulomb interaction term and the exchange interaction term, respectively [cf. Eq. (3)]. For $g_v^2 = \lambda_s^4 \equiv 1$, our variational Gutzwiller state would become equivalent to the Hartree-Fock solution ($|\psi_0\rangle = |\psi_G\rangle$), which is not the case here. More importantly, the region of maximized renormalization is located roughly around half-filling where g_v^2 is small, significantly diminishing the destructive character of the V term on the paired phase. Moreover, λ_s^4 is relatively large in the same region, which enhances the positive effect of the J term on the pairing. At the same time, since we are dealing with the weak-to-moderate correlation regime, there is no Mott insulating state located at half-filling that would suppress the SC state there. As a result, the stability of the SC state lies exactly at the crossing of the Van Hove singularity line and the maximized renormalization area at half-filling. This allows for the two positive effects to act simultaneously, which as a result create favorable conditions for the paired phase only in a particular region of the (n, D) plane. Additionally, in Fig. 3(c) we show that the SC phase vanishes while the electron-electron correlations are weakened.

For comparison, in Fig. 4 we provide the results for both weak-to-moderate and strong correlations. Namely, panels (a) and (b) correspond to $U = 80$ meV and $U = 120$ meV, respectively, while the bandwidth is $W \approx 90$ meV. In the second situation, instead of having a single SC dome, we actually obtain two of them with the SC gap reaching values one order of magnitude larger than those in the first case. This is due to the fact that for $U \gtrsim W$ strong electron-electron correlations enhance the positive effect of the renormalization parameters g_v^2 and λ_s^4 on the pairing. However, due to the fact that U is already larger than W in panel (b), a Mott insulating state starts to develop at half-filling, which suppresses the SC amplitudes there, leading to a two-dome behavior.

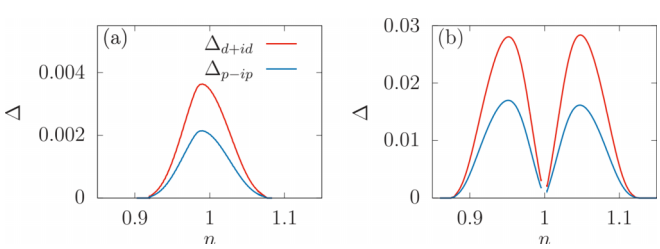

FIG. 4. Symmetry-resolved gap amplitudes of the mixed singlet-triplet solution as a function of n for $D = 0.35$ V/nm and for two selected values of the on-site Coulomb repulsion, $U = 80$ meV [panel (a)] and $U = 120$ meV [panel (b)]. In both cases, we keep $J = 4t^2/U$ and $V = U/3.635$.

It should be noted that recent measurements carried out for $\theta = 5.0^\circ$ and $\theta \approx 3.5^\circ$ twisted WSe_2 show a single SC dome not separated by a Mott state in a certain D range [16,17]. However, the original experimental report referring to the same system with a twist angle $\theta = 5.1^\circ$ shows signatures of two SC domes and a Mott insulator at half-filling [2]. It might be possible that depending on the dielectric environment and the actual twist angle the two regimes ($U \lesssim W$ and $U \gtrsim W$) can be reached in $tWSe_2$ leading to two different forms of the phase diagram. It should be noted that our results lead to a significantly larger maximal SC gap in the two-dome case, which would agree with the experimental situation where $T_C \approx 200$–300 mK and $T_C \approx 1$ K correspond to single-dome and two-dome behaviors, respectively [2,16,17]. During the resubmission process of this Letter, an experimental report has appeared [54] showing the stability of the SC phase close to the crossing between the Van Hove singularity and the half-filling, which is consistent with our approach. However, above a certain value of D, an antiferromagnetic Mott insulator begins to develop at $n = 1$.

Our Gutzwiller approach is limited to the ground state only. Therefore, we are not able to reach nonzero temperatures. Nevertheless, in order to provide a rough estimate of the maximal critical temperature in the two considered situations, we use the formulas $\Delta(T = 0) = 1.764\, k_B T_C$ and $\Delta(T = 0) = J\Delta_{\max}$, with $\Delta_{\max}$ being the maximal SC gap amplitude value obtained in our calculations. Such an estimate gives us $T_C \approx 100$ mK and $T_C \approx 450$ mK for the $U = 80$ meV (a) and $U = 120$ meV (b), respectively. The obtained values underestimate the experimentally obtained critical temperatures; however, they are of the same order.

Final remarks. We have analyzed the principal features of the unconventional superconducting state in $tWSe_2$ within an effective t-J-U model supplemented with the intersite Coulomb repulsion term. As we show, for the weak-to-moderate correlation regime the topological mixed singlet-triplet superconducting state covers a relatively small area of the (n, D) phase diagram, which is located where the Van Hove singularity line crosses half-filling. We show that this precise region optimizes the conditions for superconductivity: The VHS causes a large density of states, whereas the electron-correlation-induced renormalization is maximized at half-filling. This allows the two effects to act simultaneously, creating favorable conditions for the paired state as seen in experiments [16,17,54]. To explore the unconventional nature of the SC state experimentally, we propose using Knight shift measurements to identify any nonsinglet pairing. Observing the Kerr effect could indicate spontaneous breaking of time-reversal symmetry. Finally, our prediction of topolog-

ical superconductivity in $tWSe_2$ highlights it as a promising platform for detecting chiral edge states through scanning techniques or transport measurements [55].

Additionally, we show that a single SC dome and two SC domes can be reproduced within a single theoretical framework. The former corresponds to weaker correlations and the latter to stronger correlations. The two-dome scenario comes as a result of the fact that the Mott insulating state located at half-filling separates the SC stability range into two. Nevertheless, the maximal values of the gap amplitudes are larger for the stronger correlations and the two-dome scenario. This is in qualitative agreement with the available experimental data [2,16,17].

For the flat band of cuprate superconductors, it has been shown that the t-J-U and Hubbard models lead to a roughly similar physical picture of the superconducting phase [56]. However, since the J term does not appear explicitly in the latter, either a higher order diagrammatic expansion of the Gutzwiller wave function or a density martix renormalization group (DMRG) method would be necessary to obtain the stability of the paired phase. As we have shown very recently, the DMRG approach can indeed lead to the presence of the SC phase in the effective single-band model of $tWSe_2$ [57].

Acknowledgments. This research was funded by National Science Centre, Poland (NCN) according to decision 2021/42/E/ST3/00128. We gratefully acknowledge Polish high-performance computing infrastructure PLGrid (HPC Center: ACK Cyfronet AGH) for providing computer facilities and support within computational Grant No. PLG/2024/017372. L.R. was funded by the Swiss National Science Foundation through Starting Grant No. TMSGI2_-211296.

Data availability. The code that was written to perform the numerical calculations and the data behind the figures are available in the open repository [58].

Appendix. Here, we provide a detailed extension related to the method of determination of the superconducting gap symmetry, the influence of the spin-valley locking, and the topological features of the superconducting state.

Symmetry of the paired state. Within the presented Gutzwiller wave function approach, the unprojected wave function, $|\Psi_0\rangle$, contains the superconducting order parameter, $S_{ij}^{\sigma\sigma'} = \langle \hat{c}_{i\sigma}\hat{c}_{j\sigma'}\rangle_0$, which is related to the correlated wave function counterpart $\Delta_{ij}^{\sigma\sigma'} = \langle \hat{c}_{i\sigma}\hat{c}_{j\sigma'}\rangle_G = q^2 S_{ij}^{\sigma\sigma'}$, where $q = \lambda_s(\lambda_d n_s + \lambda_\emptyset(1-n_s))$. In our numerical scheme, we do not limit ourselves to one specific symmetry of the SC gap. Instead, we consider all possible pairing symmetries that are allowed for the case of a triangular lattice within the nearest-neighbor real-space pairing scenario. This requires solving the set of self-consistent equations for all the six complex nearest-neighbor gap amplitudes without any additional constraints. We allow for spin-singlet pairing ($S_{ij}^{\uparrow\downarrow} = -S_{ij}^{\downarrow\uparrow}$), spin-triplet pairing ($S_{ij}^{\uparrow\downarrow} = S_{ij}^{\downarrow\uparrow}$), and their mixture ($|S_{ij}^{\uparrow\downarrow}| \neq |S_{ij}^{\downarrow\uparrow}|$). We neglect the possibility of triplet $S^z = \pm 1$ pairing, as these pairing channels lead to a Fermi wave vector mismatch, which significantly suppresses superconductivity.

After we determine the gap amplitudes $\Delta_{ij}^{\bar{\sigma}\sigma}$ to all nearest neighbors, we transform them into the so-called symmetry-resolved gap amplitudes, given by

$$\Delta_{M,p}^{\sigma\bar{\sigma}} = \frac{i^p}{6}\sum_{i(j)} e^{-iM\theta_{ji}}\Delta_{ji}^{\sigma\bar{\sigma}}, \tag{A1}$$

where the summation runs over the nearest-neighbor lattice sites j surrounding site i, and θ_{ji} are angles $\{0,\ \pi/3,\ 2\pi/3,\ \pi,\ 4\pi/3,\ 5\pi/3\}$ between the positive half-x axis and the $\mathbf{R}_{ji} = \mathbf{R}_j - \mathbf{R}_i$ vector. M and p correspond to particular symmetries and are provided in Table I.

TABLE I. Symmetries of the SC gap together with their parities and Cooper pair spin state. The symmetry factor, M, and the parity factor p are provided in the first and the second column, respectively [cf. Eq. (A1)].

M	p	Gap symmetry	Parity	Spin state
0	0	Extended s	Even	Singlet
1	1	$p_x + i\,p_y$	Odd	Triplet
2	0	$d_{x^2-y^2} + i\,d_{xy}$	Even	Singlet
3	1	f	Odd	Triplet
4	0	$d_{x^2-y^2} - i\,d_{xy}$	Even	Singlet
5	1	$p_x - i\,p_y$	Odd	Triplet

Finally, we can write down the expressions for the real-space singlet and triplet gap amplitudes in the correlated state:

$$\begin{aligned}\Delta_{M,p}^{s} &= (\Delta_{M,p}^{\uparrow\downarrow} - \Delta_{M,p}^{\downarrow\uparrow})/\sqrt{2},\\ \Delta_{M,p}^{t} &= (\Delta_{M,p}^{\uparrow\downarrow} + \Delta_{M,p}^{\downarrow\uparrow})/\sqrt{2}.\end{aligned} \tag{A2}$$

For the sake of clarity, in the main text of the Letter, we use the symmetry names ($p \pm ip$, $d \pm id$, f, etc.) instead of the values of the M and p factors.

In Fig. 5, we show the $\mathbf{k}$ dependence of the SC gap corresponding to the symmetries listed in Table I. As one can see, all the symmetries fulfill the C_6 symmetry of the underlaying trianlular lattice. However, due to the presence of spin-valley locking, the Hamiltonian breaks the C_6 symmetry, which has further consequences for the pairing symmetry, as we show in the next section.

Influence of spin-valley locking on the pairing. The presence of spin-valley locking leads to two spin-split Fermi surfaces and a reduction of the symmetry from C_6 to C_3. According to our calculations, for this case, a stable SC solution corresponds to a mixed $d + id$ and $p - ip$ symmetry of the gap in the relevant range of model parameters. As one can see in Fig. 6, this particular composition of the symmetry components leads to a situation in which the SC gap fulfills the C_3 symmetry of the Hamiltonian. Moreover, there are two different SC gap distributions realized in $\mathbf{k}$ space. This allows for the SC gap to adjust to the shape of the two separate Fermi surfaces resulting from the spin-valley locking. Therefore, the mixed symmetry of the gap is a straightforward result of the spin-valley locking, which leads to reduction of the systems' symmetry and to two separate Fermi surfaces.

*Details of the topological paired state.*According to our calculations in the range of parameters corresponding to Figs. 2(e) and 2(j), the superconducting state is nontrivial topologically with the Chern number $C = \pm 4$. For clarity, we revisit here the mentioned diagram in Fig. 7. As one can see,

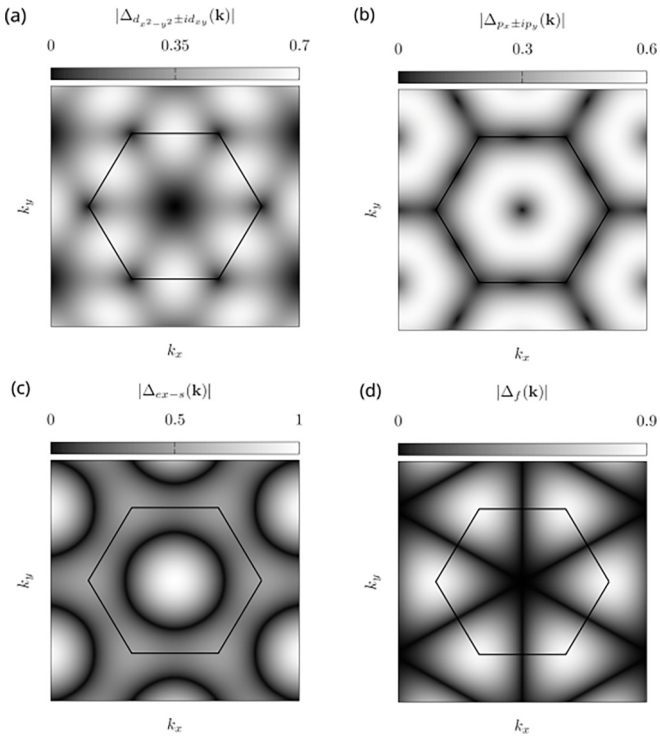

FIG. 5. The absolute value of the **k**-dependent SC gaps for the pairing channels listed in Table I. The Brillouin zone is marked by black solid line. The presented distributions have been obtained by setting particular symmetry-resolved factors to 1 and all the others to 0.

the sign change of C appears at the line representing the Van Hove singularity.

In Fig. 8, we provide the corresponding **k**-dependent SC gap as well as the normal state Fermi surfaces for two representative sets of parameters, which are marked by green dots in Fig. 7. As one can see, the obtained value of the Chern number can be understood as a total topological charge contained inside the spin-up and spin-down Fermi surfaces.

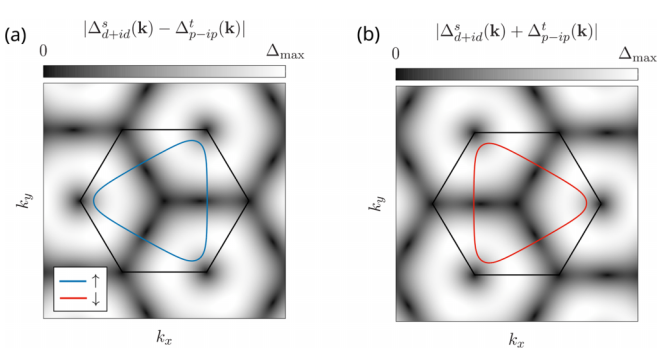

FIG. 6. The absolute value of the **k**-dependent SC gaps corresponding to mixed $d + id/p - ip$ symmetry obtained for $n = 1, U = 80\,\text{meV}$, $J = 4t^2/U$, and $D = 0.3\,\text{V/nm}$. The normal state Fermi surfaces are marked by solid blue and red lines in panels (a) and (b), respectively.

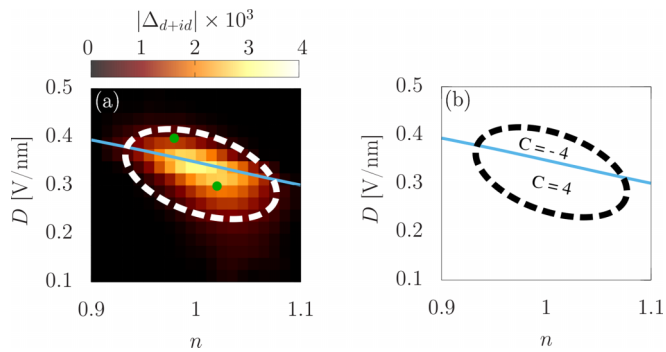

FIG. 7. (a) The SC gap amplitude as a function of band filling and displacement field for the same model parameters as in Fig. 2(e). The two green points correspond to the two representative n and D values leading to $C = \pm 4$ and selected for the detailed analysis provided in Fig. 8. (b) The phase diagram that shows the calculated values of the Chern number of the SC state.

Namely,

$$C = \sum_{i \in \Omega_{\text{FS}}} (-1)^w C_i, \tag{A3}$$

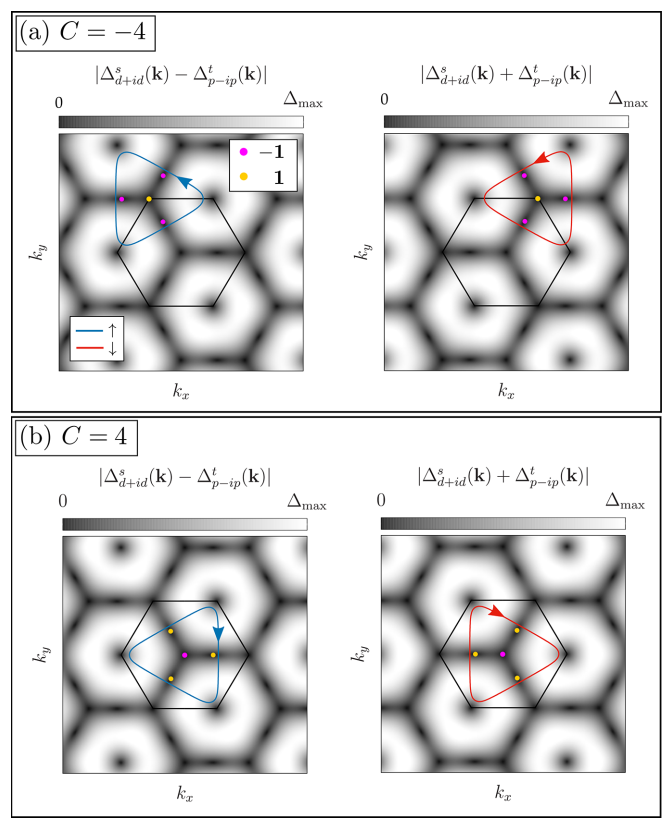

FIG. 8. The normal-state Fermi surfaces for spin-up and spin-down (blue and red solid lines) electrons as well as the **k**-dependent SC gaps for the two points marked by green dots in Fig. 7, which correspond to Chern number: $C = -4$ [panel (a)] and $C = 4$ [panel (b)]. The arrows at the Fermi surfaces represent the winding direction, which is counterclockwise (clockwise) for the electronlike (holelike) Fermi surfaces.

where C_i is the topological charge of a given nodal point, which can be determined by calculating the winding number of the order parameter around it. The sign of the Chern charge depends on whether it is enclosed by an electron- ($w = 0$) or holelike ($w = 1$) Fermi surface. The i index runs only over the nodal points that are contained inside the Fermi surface.

[1] A. Ghiotto, E.-M. Shih, G. S. S. G. Pereira, D. A. Rhodes, B. Kim, J. Zang, A. J. Millis, K. Watanabe, T. Taniguchi, J. C. Hone, L. Wang, C. R. Dean, and A. N. Pasupathy, Quantum criticality in twisted transition metal dichalcogenides, Nature (London) **597**, 345 (2021).

[2] L. Wang, E.-M. Shih, A. Ghiotto, L. Xian, D. A. Rhodes, C. Tan, M. Claassen, D. M. Kennes, Y. Bai, B. Kim, K. Watanabe, T. Taniguchi, X. Zhu, J. Hone, A. Rubio, A. N. Pasupathy, and C. R. Dean, Correlated electronic phases in twisted bilayer transition metal dichalcogenides, Nat. Mater. **19**, 861 (2020).

[3] E. Anderson, F.-R. Fan, J. Cai, W. Holtzmann, T. Taniguchi, K. Watanabe, D. Xiao, W. Yao, and X. Xu, Programming correlated magnetic states with gate-controlled moiré geometry, Science **381**, 325 (2023).

[4] Z. Tao, B. Shen, S. Jiang, T. Li, L. Li, L. Ma, W. Zhao, J. Hu, K. Pistunova, K. Watanabe, T. Taniguchi, T. F. Heinz, K. F. Mak, and J. Shan, Valley-coherent quantum anomalous Hall state in AB-stacked $MoTe_2/WSe_2$ bilayers, Phys. Rev. X **14**, 011004 (2024).

[5] E. C. Regan, D. Wang, C. Jin, M. I. Bakti Utama, B. Gao, X. Wei, S. Zhao, W. Zhao, Z. Zhang, K. Yumigeta, M. Blei, J. D. Carlström, K. Watanabe, T. Taniguchi, S. Tongay, M. Crommie, A. Zettl, and F. Wang, Mott and generalized Wigner crystal states in WSe_2/WS_2 moiré superlattices, Nature (London) **579**, 359 (2020).

[6] Y. Xu, S. Liu, D. A. Rhodes, K. Watanabe, T. Taniguchi, J. Hone, V. Elser, K. F. Mak, and J. Shan, Correlated insulating states at fractional fillings of moiré superlattices, Nature (London) **587**, 214 (2020).

[7] X. Huang, T. Wang, S. Miao, C. Wang, Z. Li, Z. Lian, T. Taniguchi, K. Watanabe, S. Okamoto, D. Xiao, S.-F. Shi, and Y.-T. Cui, Correlated insulating states at fractional fillings of the WS_2/WSe_2 moiré lattice, Nat. Phys. **17**, 715 (2021).

[8] H. Li, S. Li, E. C. Regan, D. Wang, W. Zhao, S. Kahn, K. Yumigeta, M. Blei, T. Taniguchi, K. Watanabe, S. Tongay, A. Zettl, M. F. Crommie, and F. Wang, Imaging two-dimensional generalized Wigner crystals, Nature (London) **597**, 650 (2021).

[9] H. Zhou, K. Liang, L. Bi, Y. Shi, Z. Wang, and S. Li, Spotlight: Visualization of moiré quantum phenomena in transition metal dichalcogenide with scanning tunneling microscopy, ACS Appl. Electron. Mater. **6**, 1530 (2024).

[10] T. Li, S. Jiang, B. Shen, Y. Zhang, L. Li, Z. Tao, T. Devakul, K. Watanabe, T. Taniguchi, L. Fu, J. Shan, and K. F. Mak, Quantum anomalous Hall effect from intertwined moiré bands, Nature (London) **600**, 641 (2021).

[11] Z. Tao, B. Shen, W. Zhao, N. C. Hu, T. Li, S. Jiang, L. Li, K. Watanabe, T. Taniguchi, A. H. MacDonald, J. Shan, and K. F. Mak, Giant spin Hall effect in AB-stacked $MoTe_2/WSe_2$ bilayers, Nat. Nanotechnol. **19**, 28 (2024).

[12] W. Zhao, B. Shen, Z. Tao, Z. Han, K. Kang, K. Watanabe, T. Taniguchi, K. F. Mak, and J. Shan, Gate-tunable heavy fermions in a moiré Kondo lattice, Nature **616**, 61 (2023).

[13] J. Spałek, M. Fidrysiak, M. Zegrodnik, and A. Biborski, Superconductivity in high-T_c and related strongly correlated systems from variational perspective: Beyond mean field theory, Phys. Rep. **959**, 1 (2022).

[14] Y. Cao, V. Fatemi, A. Demir, S. Fang, S. L. Tomarken, J. Y. Luo, J. D. Sanchez-Yamagishi, K. Watanabe, T. Taniguchi, E. Kaxiras, R. C. Ashoori, and P. Jarillo-Herrero, Correlated insulator behaviour at half-filling in magic-angle graphene superlattices, Nature (London) **556**, 80 (2018).

[15] Y. Cao, V. Fatemi, S. Fang, K. Watanabe, T. Taniguchi, E. Kaxiras, and P. Jarillo-Herrero, Unconventional superconductivity in magic-angle graphene superlattices, Nature (London) **556**, 43 (2018).

[16] Y. Xia, Z. Han, K. Watanabe, T. Taniguchi, J. Shan, and K. F. Mak, Superconductivity in twisted bilayer WSe_2, Nature (London) **637**, 833 (2025).

[17] Y. Guo, J. Pack, J. Swann, L. Holtzman, M. Cothrine, K. Watanabe, T. Taniguchi, D. G. Mandrus, K. Barmak, J. Hone, A. J. Millis, A. Pasupathy, and C. R. Dean, Superconductivity in 5.0° twisted bilayer WSe_2, Nature (London) **637**, 839 (2025).

[18] M. Brzezińska, S. Grytsiuk, M. Rösner, M. Gibertini, and L. Rademaker, Pressure-tuned many-body phases through Γ-k valleytronics in moiré bilayer WSe_2, 2D Mater. **12**, 015003 (2025).

[19] H. Pan, F. Wu, and S. Das Sarma, Band topology, Hubbard model, Heisenberg model, and Dzyaloshinskii-Moriya interaction in twisted bilayer WSe_2, Phys. Rev. Res. **2**, 033087 (2020).

[20] M. Bélanger, J. Fournier, and D. Sénéchal, Superconductivity in the twisted bilayer transition metal dichalcogenide WSe_2: A quantum cluster study, Phys. Rev. B **106**, 235135 (2022).

[21] L. Klebl, A. Fischer, L. Classen, M. M. Scherer, and D. M. Kennes, Competition of density waves and superconductivity in twisted tungsten diselenide, Phys. Rev. Res. **5**, L012034 (2023).

[22] F. Chen and D. Sheng, Singlet, triplet and pair density wave superconductivity in the doped triangular-lattice moiré system, Phys. Rev. B **108**, L201110 (2023).

[23] M. Zegrodnik and A. Biborski, Mixed singlet-triplet superconducting state within the moiré t–J–U model applied to twisted bilayer WSe_2, Phys. Rev. B **108**, 064506 (2023).

[24] Y.-M. Wu, Z. Wu, and H. Yao, Pair-density-wave and chiral superconductivity in twisted bilayer transition metal dichalcogenides, Phys. Rev. Lett. **130**, 126001 (2023).

[25] C. Schrade and L. Fu, Nematic, chiral, and topological superconductivity in twisted transition metal dichalcogenides, Phys. Rev. B **110**, 035143 (2024).

[26] V. Crépel, D. Guerci, J. Cano, J. H. Pixley, and A. Millis, Topological superconductivity in doped magnetic moiré semiconductors, Phys. Rev. Lett. **131**, 056001 (2023).

[27] F. Xie, L. Chen, S. Sur, Y. Fang, J. Cano, and Q. Si, Superconductivity in twisted WSe_2 from topology-induced quantum fluctuations, Phys. Rev. Lett. **134**, 136503 (2025).

[28] W. Qin, W.-X. Qiu, and F. Wu, Kohn-Luttinger mechanism of superconductivity in twisted bilayer WSe_2: Gate-tunable unconventional pairing symmetry Phys. Rev. Lett. **135**, 246002 (2025).

[29] C. Tuo, M.-R. Li, Z. Wu, W. Sun, and H. Yao, Theory of topological superconductivity and antiferromagnetic correlated

insulators in twisted bilayer WSe_2 Nat. Commun. **16**, 9525 (2025).

[30] D. Guerci, D. Kaplan, J. Ingham, J. H. Pixley, and A. J. Millis, Topological superconductivity from repulsive interactions in twisted WSe_2, arXiv:2408.16075 [cond-mat.supr-con].

[31] J. Zhu, Y.-Z. Chou, M. Xie, and S. Das Sarma, Superconductivity in twisted transition metal dichalcogenide homobilayers, Phys. Rev. B **111**, L060501 (2025).

[32] A. Fischer, L. Klebl, V. Crépel, S. Ryee, A. Rubio, L. Xian, T. O. Wehling, A. Georges, D. M. Kennes, and A. J. Millis, Theory of intervalley-coherent AFM order and topological superconductivity in $tWSe_2$ Phys. Rev. X **15**, 041055 (2025).

[33] W. Akbar, A. Biborski, L. Rademaker, and M. Zegrodnik, Topological superconductivity with mixed singlet-triplet pairing in moiré transition metal dichalcogenide bilayers, Phys. Rev. B **110**, 064516 (2024).

[34] J. Kaczmarczyk, Comparison of two approaches for the treatment of Gutzwiller variational wave functions, Philos. Mag. **95**, 563 (2015),.

[35] J. Bünemann, T. Schickling, and F. Gebhard, Variational study of Fermi surface deformations in Hubbard models, Europhys. Lett. **98**, 27006 (2012).

[36] See Supplemental Material at https://link.aps.org/supplemental/10.1103/pkf3-fkv4 for more details related to the model, method, considered pairing symmetries, and topological features of the obtained superconducting state.

[37] D. Xiao, G.-B. Liu, W. Feng, X. Xu, and W. Yao, Coupled spin and valley physics in monolayers of MoS_2 and other group-VI dichalcogenides, Phys. Rev. Lett. **108**, 196802 (2012).

[38] Y. Zhang, L. Li, J.-H. Sun, D.-H. Xu, R. Lü, H.-G. Luo, and W.-Q. Chen, Kondo effect in monolayer transition metal dichalcogenide Ising superconductors, Phys. Rev. B **101**, 035124 (2020).

[39] Y.-T. Hsu, F. Wu, and S. Das Sarma, Spin-valley locked instabilities in moiré transition metal dichalcogenides with conventional and higher-order Van Hove singularities, Phys. Rev. B **104**, 195134 (2021).

[40] J. Zang, J. Wang, J. Cano, and A. J. Millis, Hartree-Fock study of the moiré Hubbard model for twisted bilayer transition metal dichalcogenides, Phys. Rev. B **104**, 075150 (2021).

[41] F. Wu, T. Lovorn, E. Tutuc, and A. H. MacDonald, Hubbard model physics in transition metal dichalcogenide moiré bands, Phys. Rev. Lett. **121**, 026402 (2018).

[42] Y. Huang and D. N. Sheng, Topological chiral and nematic superconductivity by doping Mott insulators on triangular lattice, Phys. Rev. X **12**, 031009 (2022).

[43] S. Daul, D. J. Scalapino, and S. R. White, Pairing correlations on t–U–J ladders, Phys. Rev. Lett. **84**, 4188 (2000).

[44] S. Basu, R. J. Gooding, and P. W. Leung, Enhanced bound-state formation in two dimensions via stripelike hopping anisotropies, Phys. Rev. B **63**, 100506 (2001).

[45] E. Plekhanov, S. Sorella, and M. Fabrizio, Increasing d-wave superconductivity by on-site repulsion, Phys. Rev. Lett. **90**, 187004 (2003).

[46] T. Xiang, H. G. Luo, D. H. Lu, K. M. Shen, and Z. X. Shen, Intrinsic electron and hole bands in electron-doped cuprate superconductors, Phys. Rev. B **79**, 014524 (2009).

[47] M. Abram, J. Kaczmarczyk, J. Jędrak, and J. Spałek, d-wave superconductivity and its coexistence with antiferromagnetism in the t–j–u model: Statistically consistent Gutzwiller approach, Phys. Rev. B **88**, 094502 (2013).

[48] R. B. Laughlin, Gossamer superconductivity, arXiv:cond-mat/0209269 [cond-mat.supr-con].

[49] F. C. Zhang, Gossamer superconductor, Mott insulator, and resonating valence bond state in correlated electron systems, Phys. Rev. Lett. **90**, 207002 (2003).

[50] T. Fukui, Y. Hatsugai, and H. Suzuki, Chern numbers in discretized Brillouin zone: Efficient method of computing (spin) Hall conductances, J. Phys. Soc. Jpn. **74**, 1674 (2005).

[51] S. Raghu, E. Berg, A. V. Chubukov, and S. A. Kivelson, Effects of longer-range interactions on unconventional superconductivity, Phys. Rev. B **85**, 024516 (2012).

[52] S. Raghu, R. Thomale, and T. H. Geballe, Optimal T_c of cuprates: The role of screening and reservoir layers, Phys. Rev. B **86**, 094506 (2012).

[53] R. Nandkishore, R. Thomale, and A. V. Chubukov, Superconductivity from weak repulsion in hexagonal lattice systems, Phys. Rev. B **89**, 144501 (2014).

[54] Y. Xia, Z. Han, J. Zhu, Y. Zhang, P. Knüppel, K. Watanabe, T. Taniguchi, K. F. Mak, and J. Shan, Bandwidth-tuned Mott transition and superconductivity in moiré WSe_2, Nature **650**, 585 (2026).

[55] X.-L. Qi and S.-C. Zhang, Topological insulators and superconductors, Rev. Mod. Phys. **83**, 1057 (2011).

[56] J. Spałek, M. Zegrodnik, and J. Kaczmarczyk, Universal properties of high-temperature superconductors from real-space pairing: t–J–U model and its quantitative comparison with experiment, Phys. Rev. B **95**, 024506 (2017).

[57] A. Biborski and M. Zegrodnik, Signatures of superconducting pairing driven by electron-electron interactions in moiré WSe_2/WSe_2 homobilayer modeled by Hubbard Hamiltonian, Phys. Rev. B **112**, L161122 (2025).

[58] M. Zegrodnik, Effect of displacement field on unconventional superconductivity in twisted bilayer WSe_2 [dataset], Zenodo (2025), https://doi.org/10.5281/zenodo.15575293.